The phage L capsid decoration protein has a novel OB-fold and an unusual capsid binding strategy

Rebecca L. Newcomer [1], Jason R. Schrad [2], Eddie B. Gilcrease [3], Sherwood R. Casjens [3], Michael Feig [2], Carolyn M. Teschke [*1], Andrei T. Alexandrescu [1], and Kristin N. Parent [*2]

Affiliations

[1] University of Connecticut, Department of Molecular and Cell Biology, Storrs, CT 06269; USA

[2] Michigan State University, Department of Biochemistry and Molecular Biology, East Lansing MI, 48824; USA

[3] University of Utah School of Medicine, Division of Microbiology and Immunology, Department of Pathology, Salt Lake City, 84112; USA

Running title: Structural definition of capsid binding by Dec

* To whom correspondence should be addressed

Kristin N. Parent
Dept. of Biochem & Mol Bio
Michigan State University
603 Wilson Rd
519 Biochemistry Building
East Lansing MI, 48824

Carolyn M. Teschke
Depts of Mol and Cell Biol & Chem
University of Connecticut
91 N Eagleville Rd
Storrs, CT 06269

Key Words: bacteriophage, nanotechnology, cementing protein, capsid stability, computational modeling, β-helix

Abbreviations: cryo-EM; cryo-electron microscopy, 3DR; three-dimensional reconstruction, dsDNA; double-stranded DNA, MD; molecular dynamics, NMR; nuclear magnetic resonance, OB-fold; Oligonucleotide/oligosaccharide-Binding fold.

Abstract

The major coat proteins of dsDNA tailed phages and herpesviruses form capsids by a mechanism that includes active packaging of the dsDNA genome into a precursor procapsid, followed by expansion and stabilization of the capsid. These viruses have evolved diverse strategies to fortify their capsids, such as non-covalent binding of auxiliary "decoration" (Dec) proteins. The Dec protein from the P22-like phage L has a highly unusual binding strategy that precisely distinguishes between nearly identical three-fold and quasi-three-fold sites of the icosahedral capsid. Cryo-electron microscopy and three-dimensional image reconstruction were employed to determine the structure of native phage L particles. NMR was used to determine the structure/dynamics of Dec in solution. Lastly, the NMR structure and the cryo-EM density envelope were combined to build a model of the capsid-bound Dec trimer. Key regions that modulate the binding interface were verified by site-directed mutagenesis.

Introduction

Viral icosahedral capsids are formed from multiple copies of a single or a few types of highly structurally-conserved coat proteins that encapsidate the genome [1]. The minimum number of subunits needed to build an icosahedral capsid is 60 coat proteins, and the result is a T=1 icosahedral geometry. There is a direct correlation between genome size and T-number for dsDNA containing phages. Building a bigger capsid necessitates the use of more coat protein subunits, and requires that chemically identical proteins assemble into capsid sites with different "quasi-equivalent" conformations [2]. For example, in many of the

well-studied double stranded DNA (dsDNA) containing phages, the capsids have a T=7 geometry (see Figure 1A). These have 11 vertices formed by coat protein pentons and an additional 60 hexons to create the capsid. The 12th vertex breaks the icosahedral symmetry and is occupied by a tail that specifies host binding. Estimates predict that 10^{31} viruses are in Earth's biosphere [3,4], with dsDNA containing bacteriophages being the most abundant. These phages have an immense diversity in terms of size and complexity. The highly ubiquitous HK97-like fold is the building block for virtually all dsDNA containing phages, and allows for enormous versatility in icosahedral geometry, that can lead to differences in biophysical properties [5]. To withstand environmental stresses and the internal pressure that amasses as a result of dsDNA genome packaging, some dsDNA phages encode additional "decoration" proteins that bind to the exterior of their capsids and stabilize the virions. How various decoration proteins recognize and bind to specific sites on capsids with different icosahedral geometries is, however, still poorly understood.

The tight packing of the dsDNA genomes into the virions of many phages and herpesviruses creates enormous internal pressure (10 - 60 atm) within the capsids, resulting in high-energy states that prime the particles for infection, and facilitate delivery of the majority of the viral genomes into the hosts [6-13]. Phages have evolved diverse strategies to strengthen their capsids against the internal pressures resulting from genome packaging. In the well-studied phage HK97, the coat proteins form covalent crosslinks [14] with neighboring subunits, thereby creating a unique "chainmail" lattice [15,16]. By contrast in some other phages, a separately expressed auxilliary "decoration" protein (sometimes called "cementing" protein) functions as a molecular staple to stabilize the mature capsids. The essential phage λ decoration protein gpD stabilizes its capsid [17,18] and binds at all possible binding sites between capsomers including positions at both icosahedral and local three-fold symmetry axes [19-21]. Other related phages do not utilize covalent crosslinks for stability, or auxillary decoration proteins. Instead, these capsids rely entirely on stabilizing

85 interactions between protein subunits. For example, a portion of the coat protein called the
86 "P-loop" (see Supplementary Materials Figure S2) can create stabilizing interactions with
87 neighboring capsid subunits around three-fold symmetry axes in the absense of auxiliary
88 decoration proteins for many diverse phages [22-26].

89 Bacteriophages P22 and L are members of the short-tailed phages (family
90 *Podoviridae),* in the sub-group of P22-like phages [27]. Phage P22 is a particularly well-
91 studied model for understanding the biophysical mechanisms of capsid assembly [28] and
92 capsid protein structures at near-atomic level detail [29,30]. The coat proteins of the P22-like
93 phages, like all known tailed phages and herpesviruses, share a canonical HK97-like coat
94 protein fold, one of the most ubiquitous protein folds in nature [31,32]. The coat proteins of
95 phage L and phage P22 share 99.6% identity with only 4 amino acids differing out of 430,
96 but only phage L encodes the small auxillary decoration protein, Dec [33]. Phage L and P22
97 encapsidate similar length genomes and have similar capsid diameters. Therefore, the
98 internal pressures within both capsids are likely to be similar. Dec binds to P22 capsids *in*
99 *vitro* with nanomolar affinity at the same sites as on phage L virions, and increases the
100 stability of P22 capsids at elevated temperatures when treated with a Mg^{++} chelator *in vitro*
101 [33,34]. Thus, the role(s) of Dec in the life cycle of phage L compared to P22 is not
102 immediately obvious, and, unlike gpD in phage λ, Dec is not essential to withstand genomic
103 packaging forces in phage L virions (E. Gilcrease and S. Casjens, unpublished). The
104 reasons why some phages require stabilization mechanisms such as decoration proteins,
105 and others do not, despite using highly similar functional capsid building blocks remain
106 poorly understood.

107 Like phage λ's cementing protein gpD, phage L's Dec binds as a homotrimer only to
108 mature particles, and not precursor procapsids [33]. This indicates the proteins are not
109 involved in capsid assembly but recognize specific surface topology features of mature

capsids. During maturation, dsDNA-containing phage and herpesvirus capsids undergo expansion and massive conformational changes, stabilizing the particles and exposing new residues to the surface [23,29,35]. The T=7 organization of P22 and phage L capsids results in different protein landscapes between neighboring capsomers due to the previously described 'quasi-equivalence' constraints (Figure 1A). At the center of each of the capsid's 20 icosahedral facets there is a highly symmetric trimeric interaction formed by the three surrounding hexons (called the "icosahedral three-fold" axis; black triangle in Figure 1A). Between other hexons there are "quasi-three-fold" symmetry axes (magenta circles in Figure 1A), which have a sublty different arrangement than the icosahedral three-fold symmetry axes. These quasi-three-fold sites are less symmetric, and have bent contacts between capsomers when compared with an icosahedral-three-fold symmetry site. Lastly, there is a second type of quasi-three-fold symmetry site that occurs between hexons and the pentons (green triangles in Figure 1A). Tight binding (~nM affinity) of Dec occurs at only quasi-three-fold axes between hexons (magenta circles). In contrast to other types of cementing proteins, binding of Dec to the 20 "true" icosahedral three-fold symmetry axes (black triangles in Figure 1A) occurs only weakly. The binding affinity for the true three-folds is at least an order of magnitude lower than for the quasi-three-folds [36], so that the former sites are very sparsely occupied by Dec on the native phage L particles. No binding has been detected at the quasi-three-fold sites surrounding the pentons (green circles) [34,36]. Dec's ability to bind discriminately is in sharp contrast with the decoration proteins of other phages that fully saturate all symmetry-related sites in mature virions.

Defining the mechanisms by which different decoration proteins, such as gpD and Dec, bind viral particle surfaces is not only important for understanding the underlying biology, but is also critical for (1) the potential exploitation of phages in nanomedicine [37-40], (2) structure-guided design of virus-inspired nanomaterials [10,36,41-44], and (3) sheding light on capsid assembly and stabilization processes [29,45]. Here, we investigate

136 how Dec is able to distinguish subtly different capsid binding sites with high specificity.
137 Furthermore, we report the structure of phage L Dec protein, which has a novel fold for a
138 decoration protein. We used a combination of structural approaches to understand how Dec
139 interacts with phage capsids including (1) cryo-electron microscopy (cryo-EM) and three-
140 dimensional image reconstructions (3DR) of native phage L particles, (2) Nuclear Magnetic
141 Resonance (NMR) structure and dynamics of Dec in solution, and (3) computational
142 modeling of the Dec trimer. Dec displays significant asymmetry and flexibility when bound to
143 capsids. The N-terminal globular domain of the protein that contacts the capsid has an
144 Oligonucleotide/oligosaccharide-Binding structure (OB-fold; [46]), and the C-terminal portion
145 of Dec is comprised of a putative three-stranded β-helix domain. Several key residues within
146 both the phage L coat protein lattice and the Dec trimer are predicted from our structural
147 model to modulate the affinity of Dec binding. The contributions of these residues towards
148 Dec binding were probed by site-directed mutagenesis. Our findings reveal that Dec uses a
149 binding mechanism that is not shared by other known phages and viruses, uncovering new
150 insights into phage biology and stabilization mechanisms. The combination of these results
151 provides a highly tunable and novel platform for future uses in virus-inspired nanodesign.
152

153 **Results**

154 **Cryo-EM structure of phage L at near-atomic resolution:**

155 As a first step towards understanding the mechanism by which Dec binds to phage L,
156 we determined the structure of native phage L capsids using cryo-EM (Figures 1 & S1).
157 Local resolution analysis [47] shows that some areas of the map are better resolved than
158 others, such as the capsid proteins and the base of the Dec trimer, whereas the distal end of
159 Dec is at much lower resolution (Figure S1C). Both the overall protein structure, as well as
160 the specific contact points for attachment of Dec trimers to the coat protein subunits are
161 clearly discernable near quasi-three-fold symmetry axes between hexons. As anticipated

162 from previous studies [34,36], Dec very sparsely occupied icosahedral three-fold symmetry
163 sites in phage L virions (data not shown), as there was only a hint of very weak density
164 observed at these positions, and no Dec occupancy was observed at the alternative quasi-
165 three-fold sites between hexons and pentons (Figure 1A). Segmentation of the Dec density
166 from the virion density map for subsequent analysis was performed using UCSF Chimera's
167 Segger [48] (Figure 1B, C).
168
169 **Structures of the phage L coat lattice and capsid-bound Dec trimer:**
170 As an initial guide for accurately fitting the phage L coat protein into the cryo-EM
171 density, we used the most recent 3.3 Å-resolution structure of phage P22 coat protein (PDB
172 ID: 5UU5; [49]), since phage L and phage P22 are highly homologous, differing at only four
173 positions of their 430 amino acid coat proteins [34]. Upon initial docking, we found small
174 discrepancies between the phage L capsid cryo-EM density and the P22 coat protein
175 asymmetric unit structure. Therefore, to optimally fit the cryo-EM density we refined the
176 phage L asymmetric unit where each capsid protein was allowed to move independently in
177 the cryo-EM density envelope using Phenix (Table 1). The phage L capsid protein subunit
178 domains (Figure S2) are named as defined for P22 coat protein [49,50]. The four amino acid
179 sequence differences between phage L and P22 coat proteins were accounted for during
180 modeling and are not near the Dec binding interface (see Movie S1). The R101H difference
181 is within the spine helix pointing towards the capsid interior, I154L is located in the A-domain
182 towards the hexamer center, M267L is in the I-domain, adjacent to but not interacting with
183 Dec, and A276T in also located in the I-domain but on the distal end pointing towards the
184 center of the hexamer (Figure S2). Overall, there were only very minor differences between
185 the optimally fit P22 and phage L capsid lattices. The phage L coat protein (Cα backbone)
186 deviated from those in the P22 structure (PDB 5UU5) by about 1 Å for the hexamer and 1.5

187 Å for the penton unit, which is in the range of what may be expected for structures of
188 homologous proteins [51].

189 At lower resolution, the capsid-bound Dec trimer was previously reported to have a
190 tripod shape with three N-terminal legs interacting with the capsid surface, and a protruding
191 central C-terminal head or stalk [34,36]. Our results agree with the previously published
192 structure, however the higher-resolution structure of Dec, particularly in the N-terminal
193 region, now allows a detailed analysis of the fold of the protein and interpretation of the
194 binding interface. The trimeric Dec density (one segmented trimer shown in Figure 1B) is
195 asymmetric and well defined at the quasi-three-fold symmetry axes between hexons [36,42].
196 The resolution within the Dec density is on average lower than the capsid, likely due to
197 protein flexibility, especially in the C-terminal stalk region (Figure S1C).

198

199 **The NMR structure of the Dec monomer consists of an OB-fold domain and an**
200 **unfolded C-terminus:**

201 To investigate the properties of free Dec in solution, we used NMR to characterize
202 the unassembled protein in the absence of capsids using an acid unfolding protocol of
203 lowering the pH to 2, followed by a refolding step induced by adjusting the pH to 4 as
204 defined in [52]. Subsequent characterization of the protein using size exclusion
205 chromatography, native-gel electrophoresis, and ^{15}N NMR relaxation measurements (Figure
206 S3) showed that the unfolding/refolding protocol converts purified Dec from a trimer to
207 partially folded monomers [52]. The high quality of the NMR data enabled us to obtain nearly
208 complete (98%) NMR assignments for the monomeric Dec protein [52]. The NMR structure
209 was determined using the program ARIA 2.3 [53], based on the experimental NMR
210 constraints summarized in Table 2. The coordinates of the Dec monomer NMR structure
211 ensemble have been deposited to the PDB under accession number 6E3C.

The N-terminal domain of the Dec monomer has an OB-fold motif (Figure 2). The final NMR structure (Figure 2A) is close to an initial NMR model calculated with the program CS-ROSETTA [54], based on the assigned NMR chemical shifts in combination with template-based modeling (Figure S4). The backbone (Cα, C', N, O) RMSD is 2.3 Å over the folded parts of the structure (residues 12-89) between the NMR structure and the CS-Rosetta model. Submission of the NMR Dec monomer structure to the DALI server [55] identified about 80 matches to proteins that contain similar OB-fold domain structures. The strongest of these is a portion (residues 117-174) of chain E of the 40S ribosomal protein SA (PDB code 4KZX-E). This superposed on the Dec NMR structure with a Cα RMSD of 3.5 Å over 61 residues, supporting our interpretation that the structure of the Dec N-terminus is in the OB-fold family.

The canonical OB-fold motif [46] is a five-stranded Greek key β-barrel, comprised of a β1-β3 meander and a β4-β5 hairpin, with an α-helix 'αOB' intervening between strands β3 and β4. The five-stranded OB-fold β-barrel is closed by an antiparallel pairing between strand β1 and β4, and a short parallel pairing between stands β3 and β5 [46]. In the Dec structure the anti-parallel pairing of stands β1 and β4 is conserved, but strands β3 and β5 are too distant (~13 Å) for any H-bond contacts. Thus, the Dec β-sheet is distorted to a more open structure compared with the classical five-stranded OB-fold β-barrel (Figure 2B). In general, the cores of OB-fold β-barrels are consolidated by three layers of hydrophobic residues [46,56]. This arrangement is also present in the Dec structure (not shown). The canonical role of the helix αOB is to provide a 'hydrophobic plug' for the bottom hydrophobic layer of the β-barrel [46,56]. Residue V55 appears to serve this role in Dec. In OB-fold proteins the orientation of the helix αOB is more variable than that of the β-barrel [57,58], and in Dec, the αOB helix extends almost directly between strand β3 and β5, with the helix axis in the plane of the β1-β3 meander, rather than below this structure (Figure 2B).

237 As with many OB-fold proteins [58], Dec has additional non-conserved elements of
238 secondary structure at the periphery of the conserved motif. The short strand β0 forms an
239 anti-parallel pair with the N-terminus of the OB-fold strand β1, and the helix αC extends
240 away from the last OB-fold strand β5 (Figure 2C). Outside of the folded globular part of the
241 Dec monomer structure, residues 1-11 and 90-134 are disordered (Figure 2B). Although
242 these segments were included in the NMR structure calculations, they have no defined
243 structure in the Dec monomers (Figure 2B).

244 To further characterize Dec, we analyzed the dynamics of the monomeric protein
245 using NMR ^{15}N-relaxation data in terms of the "Model-Free" formalism (Figure S3). The local
246 backbone mobility of the Dec monomers is summarized in Figure 3. The N-terminus from
247 residues 1-11 and the C-terminus from residues 90-134 have small S^2 order parameters
248 characteristic of unfolded protein segments (Figure 3A, Movie S3). The random coil
249 chemical shifts of these regions [52] and the lack of long-range NOEs, are also consistent
250 with these segments being unstructured in the Dec monomers. Small and intermediate S^2
251 values indicative of increased flexibility on the ps-ns timescales are also seen at sites within
252 the folded globular portion of Dec (Figure 3A). Information on motions within slower μs-ms
253 timescales can be garnered from exchange contributions to R2 transverse relaxation ($R2_{EX}$
254 parameters). The sites with the largest $R2_{EX}$ contributions are similar to those with low S2
255 order parameters, in particular loops L2-3, L4-5 and the region surrounding the loop L3-
256 α (purple and red in Figure 3B). The sites within the folded portion of the Dec monomers
257 with the largest flexibility based on S^2 and $R2_{EX}$ values are shown in Figures 3 C, and D,
258 respectively.

259

260 **Homology modeling of phage-bound Dec suggests a trimeric β-helix motif forms the**
261 **C-terminal spike:**

262 The NMR structure of Dec revealed an OB-fold for the N-terminal portion of the
263 protein; however, the C-terminal portion was unstructured for the monomer in solution. As
264 we previously observed [36], the N-terminal domain forms the legs of the Dec "tripod" that
265 are bound to the capsid, and the C-terminal region forms its protruding central stalk. The
266 ordered N-terminal domain was not sufficient to fill the entire density within the cryo-EM map.
267 Moreover, fitting the N-terminal folded OB-fold into the density showed little or no inter-
268 subunit trimer contacts from the first 77 residues of Dec. Thus the C-terminus of Dec,
269 evident as a spike in cryo-EM maps of capsid bound Dec [36], becomes ordered either upon
270 Dec trimerization or capsid binding.

271 We used a combination of the NMR structure and homology modeling to build a
272 model of the capsid-bound Dec trimer using the cryo-EM density map as a guide. We initially
273 docked the NMR derived OB-fold portion of the Dec structure (residues 10-77) into the
274 segmented cryo-EM density, independently fitting three copies of the OB-fold. Using Phenix,
275 each copy was refined by flexible fitting to accommodate the slight differences in the
276 asymmetric trimer density. We then built a complete trimer by using a combination of
277 homology modeling and flexible fitting to refine the C-terminal portion of Dec separately from
278 that of the OB-fold. Homology of the C-terminus most closely matched a fragment from the
279 bacteriophage T4 trimeric proximal long tail fiber protein gp34 (PDB ID: 4UXE [59]) (see
280 Materials and Methods for details), and was fit to the segmented cryo-EM density. In brief,
281 the C-terminal domain (residues 78-134) was modeled as a three-stranded β-helix domain
282 based on the remote homology model, consistent with predicted secondary structures of the
283 tail fiber protein gp34, and to fit the cylindrical shape of the cryo-EM density for the C-
284 terminal domain. The C-terminus of the final trimeric Dec structure was then further refined
285 using partially flexible fitting preserving the β-helix domain as a rigid unit within the cryo-EM
286 density envelope (Figure 4). These residues are predicted with a lower confidence owing to

287 the flexibility and lower resolution within that portion of the structure and were refined using
288 the Cα backbone only in this region.
289
290 **Mutagenesis of P22 coat protein and Dec reveals key residues that modulate binding:**
291 The OB-fold of Dec, as determined by NMR, fits the cryo-EM map of the "tripod" legs
292 in the native phage L virion very well (Figure 4). This allowed us to fit models of several coat
293 protein subunits and Dec to analyze the Dec-coat protein binding interface. The resolution of
294 the coat protein in the cryo-EM map in this region was sufficient to fit some bulky side chains.
295 Furthermore, the NMR structure allowed us to make predictions regarding the side chain
296 orientation of Dec residues that potentially bind to coat protein. Analysis of the binding
297 interface revealed several residues in close contact between the phage L coat protein and
298 Dec that appear to be important for binding. Therefore, we tested our models using site-
299 directed mutagenesis of phage P22 coat protein. P22 is a very well-established model
300 system with a variety of molecular tools readily available [29]. Previous work has shown that
301 P22 and phage L behave similarly [33,34,36] and all of the amino acid substitutions found in
302 phage L have even been identified occasionally in P22 stocks as phenotypically silent
303 mutations (Teschke lab, unpublished data). Lastly, as Dec bound to P22 is a widely used
304 system for a variety of nanomaterials applications [10,42,43], identifying key residues that
305 contribute to Dec interactions with P22 is highly useful for practical applications. Therefore,
306 we felt it reasonable to use the established genetics of P22 as a model for the native phage
307 L for our mutagenesis studies.
308 Previous work suggested that Dec binding to P22 capsids is driven primarily through
309 electrostatic interactions [42], and our data also suggest a charged binding interface. To
310 assess the role of specific coat protein surface residues in modulating Dec binding, the
311 following five coat protein residues in potential close contact with Dec were chosen for
312 single amino acid substitution by site directed mutagenesis: E81R, P82S, R299E, P322S,

313 and E323R (Figure 5; Supplementary Materials, Movie S2). Site directed mutagenesis was
314 performed on a plasmid that expresses coat protein (see Materials and Methods) as
315 described previously [60-62]. Cells carrying the plasmid were infected with phages having a
316 nonsense mutation in gene *5* (encodes coat protein), so that any phages produced are the
317 result of complementation by the coat gene expressed from the plasmid. None of the amino
318 acid substitutions affected virion production or infectivity; phages assembled with each coat
319 protein variant were grown to high titer and were phenotypically indistinguishable from the
320 parental phage.

321 Coat proteins occupying different local conformations (as a result of the quasi-
322 equivalent capsid lattice) contribute different residues to the binding interface (Figure 5A,
323 Movie S2). For example, residues E81, P82, and R299 from the coat protein subunits that
324 form the quasi-three-fold symmetry axes (grey subunits in Figure 5) contact Dec, whereas
325 residues P322 and E323 contact Dec from adjacent and overlapping coat protein subunits
326 (black subunits in Figure 5). To assess the role that specific Dec residues play in capsid
327 binding, we also made five single amino acid substitutions in recombinant Dec protein:
328 K30D, Y31A, Y49E, Y71A, and E73R (see Materials and Methods). Modified Dec proteins
329 were added to mature WT phage particles, complexes were purified using CsCl gradients,
330 and relative amount of each Dec protein bound to virions was quantitated. The global
331 secondary structure of all Dec variants was indistinguishable from the WT protein by circular
332 dichroism. Furthermore, native gel experiments performed as described previously [52]
333 showed that all Dec variants assemble as trimers in solution. Therefore any changes in Dec
334 occupancy in the variants are likely due to a disruption of the binding interface, rather than
335 protein folding artifacts.

336 Among the five coat protein changes, coat amino acid substitutions E81R and
337 E323R attenuated but did not completely abolish Dec binding ability (Figure 5B, C). We
338 created a variant containing both amino acid substitutions, E81R:E323R, which displayed

339 less Dec binding (<20%) than each of the individual substitutions. Since the E81R:E323
340 double mutant affects both Dec binding sites, our data indicate that the binding interface
341 involves more than these two residues. It is also possible that given the inherent asymmetry
342 in the capsid quasi three-fold binding sites for Dec because they are formed by coat proteins
343 in two distinct quasi-equivalent conformations, not all chains of the Dec trimer have equal
344 effects form the amino acid substitutions. Dec with amino acid substitutions K30D and Y49E
345 displayed lower binding than the WT protein, consistent with the prediction of an
346 electrostatic binding interface (Figure 5D, Movie S2).

347 The close contact region between Dec and coat can be thought of as including two
348 binding sites. One site includes coat residues E81 and P82 that interact with Dec residues
349 K30, Y31 and Y49 (Figure 5D, "site 1"). Dec residue Y49 is directed towards the side chain
350 of coat residue E81. The other site includes Dec residues Y71 and E73 and coat residues
351 P322, E323 and R299 (Figure 5D, "site 2"). Overall, variations in site 1 had the largest effect
352 on binding. In Dec, site 1 residues K30 and Y49 had the largest effect on binding saturation,
353 and in coat protein site 1 residue E81R had the largest effect relative to the other
354 substitutions. Although site 1 clearly plays a strong role in modulating Dec binding, coat
355 residue E323R that occupies site 2 had a modest but reproducible effect. We conclude that
356 the site 1 plays a larger role in mediating Dec binding to coat protein, and is largely due to
357 electrostatic interactions.

358 We also tested our hypothesis by making substitutions in residues near sites 1 and 2.
359 As expected, these did not reduce binding (namely coat residues P82S, R299E and P322S;
360 we intentionally made conservative proline substitutions as coat protein is highly
361 aggregation prone [29]). Similarly changes in nearby residues in Dec also did not reduce
362 binding, including Y31A, Y71A, and E73R. These observations are consistent in light of the
363 3D capsid structure, and indicates that sites 1 and 2 are the true binding sites.
364

365 **Discussion**

366

367 **Decoration proteins employ a variety of binding schemes to adhere to phage capsids:**

368 For dsDNA tailed phages and related viruses, decoration proteins can occupy the
369 capsid lattice in several different positions. Some decoration proteins bind capsids at the
370 center of hexamers including those of phages T4, T5, RB49, and Sf13 through Sf19, [63-66].
371 Other decoration proteins bind the edges of hexamers as exemplified by gp17 in phage N4
372 [67]. Finally, there are decoration proteins that bind the capsid in areas between capsomers
373 such as gpD in λ, gp56 in phage TW1, Soc in phage T4, gp87 in phage P74-26, and Dec in
374 phage L [20,34,68-70]. In all of the aforementioned cases, the decoration proteins are added
375 after capsid assembly. Conversely, the herpesvirus heterotrimeric triplex protein decorates
376 the outside of the capsid and is also essential during capsid assembly [71,72]. For the
377 majority of these examples, all possible quasi-equivalent binding sites on the lattice are
378 occupied by the decoration proteins. By contrast, in phage L, Dec uniquely binds at one type
379 of symmetry axis with high affinity: the quasi-three-fold sites between hexamers (Figure 1A).

380 To function in a stabilizing capacity, decoration proteins must bind capsids with high
381 enough affinity to remain associated even under harsh environmental conditions. As
382 described above there are many potential binding sites on capsids, so the requirement for
383 Dec binding affinity must be balanced against binding specificity, to allow discrimination
384 between binding sites. Indeed there is a wide range of reported K_Ds for various decoration
385 proteins. Phage L's Dec and T4's Hoc bind their respective capsids with nM affinity, whereas
386 pb10 binds phage T5 with pM affinity [36,63,73]. Taken together, variations in binding
387 affinities and saturating versus discriminating binding behavior suggests that decoration
388 proteins are capable of recognizing subtle differences in capsid lattices. The reason some
389 decoration proteins evolved to discriminate between similar quasi-equivalent sites is
390 unknown, but at some positions on the capsid lattice coat-coat interactions may be stronger

391 than at other quasi-equivalent positions; therefore, some positions may not require
392 stabilization from a decoration protein. Yet, other positions may be more vulnerable to
393 environmental assaults than others, and benefit from additional stabilization.

394 How might Dec discriminate between the different three fold sites on phage L?
395 Figure 6 shows a comparison of the coat protein subunits surrounding two types of quasi
396 three-fold axes. Coat residues that interact with Dec, in particular E81 (see above), shows a
397 substantial difference in position at these difference capsid locations. These coat protein
398 topology differences are likely responsible for the failure of Dec to bind to the type of quasi
399 three-fold site surrounding pentamers and the different Dec binding affinity from the
400 icosahedral three-fold site as measured *in vitro* [36]. The coat protein subunits surrounding
401 the quasi three-fold symmetry axes between pentamers and hexamers (green circles in
402 Figure 1A) that do not bind Dec have the greatest surface curvature with highly bent
403 contacts between capsomers (Figure 6). These interfaces are a weak point in many capsids
404 as perturbations such as chemical or thermal treatments can cause entire pentamers to be
405 released from the capsid [36,74]. The quasi-three fold coat protein subunits between
406 hexamers that do bind Dec also have some curvature, but it is less extreme than the quasi
407 three folds between pentamers and hexamers (Figure 6), likely why Dec can bind here,
408 albeit at orders of magnitude lower affinity [36]. By contrast, the icosahedral three-folds sites
409 are the flattest, and although some capsids use decoration proteins to stabilize this interface,
410 Dec is not used this way in native phage L particles. Biophysical measurements have shown
411 that Dec plays a much larger role in stabilizing dsDNA-containing heads compared to empty
412 capsids, and atomic force microscopy experiments showed Dec binds the capsid at
413 positions that can suffer mechanical damage [75]. Therefore, Dec binds specifically at the
414 quasi three-fold axes between hexamers via specifics residues within the key binding site
415 (Dec site 1), and displacement of the corresponding binding partner residues within the
416 capsid lattice decreases binding affinity at other capsid locations.

417

418 **Dec has a novel architecture:**

419 In dsDNA-containing tailed phages, previously studied decoration proteins for which
420 atomic-resolution structures are known have two basic types of protein folds. Decoration
421 proteins such as phage T5's pb10 and T4's hoc, have an overall Ig domain fold [63,66]. A
422 second, more common type of decoration protein, exemplified by phage lambda's gpD, P74-
423 26's gp87, phage 21's SHP, and TW1 gp56, have similar polypeptide folds and form a
424 symmetric trimer with an N-terminal β-tulip domain and an α/β subdomain that binds and
425 stabilizes capsids through hydrophobic interfaces [70,76]. Our work shows that Dec
426 represents a third type of decoration protein fold (Figure 6), the OB-fold, as well as a
427 different capsid-binding mechanism that discriminates against quasi three-fold capsid
428 binding sites between pentamers and hexamers as well as that at the icosahedral three-fold
429 sites. To our knowledge, Dec represents the first occurrence of an OB-fold structure in a
430 virus decoration/cementing protein. Dec may have additional functions besides capsid
431 stabilization. For example, Dec could play a role in cell adhesion. Preliminary evidence
432 suggests that Dec might bind to target cells, presumably through carbohydrate moieties
433 emanating from the target cell surfaces (Teschke lab, unpublished data). From a structural
434 point of view, both the OB-fold part of Dec and the C-terminal beta-helix could be
435 carbohydrate-binding motifs. However, future work will be needed to fully explore and
436 validate this hypothesis. If Dec plays a role in cell surface binding, 60 Dec trimers rather
437 than the saturating 140 must be sufficient for this function.

438

439

440 **Dec binds phage L capsids with an unusual strategy:**

441 Crystal structures for gpD [77], gp87 [70], and SHP [78] lack resolution for several N-
442 terminal residues, indicating that these regions are flexible when these decoration proteins

443 are not associated with capsids. Cryo-EM maps of gpD in native phage λ show that the N-
444 terminus becomes highly ordered when gpD is in a bound conformation, and that the N-
445 terminus is the major part of the capsid binding mechanism as the N-terminus forms a
446 stabilizing β-sheet with strands supplied from the capsid protein [20]. Like gpD, the N-
447 terminus of the Dec monomer is disordered in solution as shown here by NMR. However,
448 unlike gpD, our data indicates that the Dec N-terminus remains rather flexible in the capsid-
449 bound form since there is (1) no cryo-EM density that is attributable to the first 10 residues,
450 (2) our previous cryo-EM data show the N-terminus of Dec can be labeled with large cargo
451 such as nanogold beads that are rather flexibly bound to the capsid [36], and (3) deletion of
452 the first 11 residues of Dec does not affect capsid binding affinity [42]. When we compare
453 the phage L Dec binding motif to the capsid stabilization mechanism in HK97, we see that
454 the residues that control Dec binding occupy similar spatial positions as the HK97
455 crosslinking residues that crosslink to form the lattice "chainmail", suggesting that
456 stabilization at this type of interface is crucial to capsid stability.

457 Furthermore, comparison of Dec to the β-tulip family of decoration proteins highlights
458 some interesting implications about binding affinity and selectivity of binding locations in
459 terms of symmetry of the auxiliary proteins involved. Perfect trimeric symmetry in a bound
460 decoration protein may allow a broader binding specificity. For example, gpD and gp87 are
461 highly symmetric trimers and these decoration proteins occupy all quasi-equivalent binding
462 sites including icosahedral three fold symmetry axes and also both types of quasi-three-fold
463 sites. By contrast, the asymmetry in the bound Dec trimer evinced by cryo-EM is an unusual
464 property among decoration proteins and correlates with its binding selectivity to only the
465 quasi three-fold sites between hexamers. Dec appears to represent a separate evolutionary
466 lineage of decoration proteins that is distinctly different than those in the β-tulip family and

467 whose capsid binding is similarly driven mainly by interactions in site 1, with a smaller
468 contribution towards binding in site 2.
469
470
471 **Materials and Methods**
472
473 **Strains and media:** Phage L, its bacterial host, and purification procedures to produce high-
474 titer stocks were previously described [33,34]. Stocks were stored in a 10 mM Tris (pH 7.6)
475 and 10 mM $MgCl_2$ buffer. LB Miller broth and LB agar (Invitrogen) were used for all
476 experiments.
477
478 **Purification of P22 phage with various coat proteins:** *Salmonella enterica* serovar
479 Typhimurium strain DB7136 (leuA414am, hisC525am, su^0), expressing P22 coat protein
480 from mutant pMS11 plasmids, were infected with P22 phage carrying amber mutations in
481 gene *5* to stop production of phage-encoded coat protein as described previously [62]. This
482 P22 strain also carried the c1-7 allele to prevent lysogeny. The resulting phages containing
483 amino acid substitutions in coat protein were purified using standard protocols [33,36].
484
485 **Site-directed mutagenesis of P22 coat protein and phage L Dec protein:** The plasmid
486 pMS11 was mutated using Quikchange protocols as described previously [79] to generate
487 plasmids that express coat protein containing the following substitutions: E81R, P82S,
488 R299E, P322S, E323R, E81R:E323R. All plasmids were Amp^R (100 μg/mL) and IPTG
489 inducible (1 mM). Sequences were confirmed at the RSTF Genomics Core at Michigan
490 State University. Plasmid pDec was mutated using Quikchange protocols, and was used to
491 express wild type and variant Dec, each with a C-terminal histidine tag. Phage P22
492 purification [33,36] and binding assays were performed as described [34,36]. To measure

493 binding, purified Dec was added to P22 phages made with WT or variant coat proteins. Free
494 Dec was separated from Dec bound to P22 particles by cesium chloride density gradient
495 sedimentation as previously described [33,34]. Bands containing P22 were TCA-precipitated,
496 and analyzed by SDS-PAGE. Coomassie-stained gel bands corresponding to P22 coat
497 protein and Dec were quantitated and normalized to the ratio found in native P22 particles
498 when bound with Dec. All binding experiments were repeated two to four times.
499 Representative data are shown.
500

501 **Cryo-EM:** Aliquots (~5 μL) of phage L virions were vitrified and examined using published
502 procedures [80]. Briefly, this involved applying samples to Quantifoil R2/2 holey grids that
503 had been plasma cleaned for ~20 sec in a Fischione model 1020 plasma cleaner. Grids
504 were then blotted with Whatman filter paper for ~5 sec, and plunged into liquid ethane.
505 Samples were pre-screened for concentraton and purification quality in a JEOL JEM-
506 2200FS TEM using a Gatan 914 specimen holder, using standard low-dose conditions as
507 controlled by SerialEM [81]. High-resoluiton imaging on an FEI Titan Krios was performed at
508 Florida State University. Micrographs were recorded on a Direct Electron DE-20 camera wth
509 a capture rate of 25 frames per second using a total of 53 frames, and a final dose of ~27
510 e/Å^2 at a final pixel size of 1.26 Å. Movie correction was performed using the Direct Electron
511 software package, v2.7.1 [82] on entire frames.
512
513 **3D image reconstructions of icosahedral particles:** Micrographs exhibiting minimal
514 astigmatism were selected for further processing. The objective lens defocus settings used
515 to record each data set ranged 0.35 to 2.49 μm. In total, the final reconstruction used 7,879
516 of the best particles from 494 images. The program RobEM
517 (http://cryoEM.ucsd.edu/programs.shtm) was used to estimate micrograph defocus and

518 astigmatism, extract individual phage L particles, and to preprocess the images. 150 particle
519 images were used as input to the random-model computation procedure to generate an
520 initial 3D density map at ~25 Å resolution [83]. Each map was then used to initiate
521 determination and refinement of particle orientations and origins for the complete set of
522 images using the current version of AUTO3DEM (v4.01.07) [84]. Phases of the particle
523 structure factor data were corrected to compensate for the effects caused by the microscope
524 contrast-transfer function, as described [85]. The Fourier Shell Correlation ($FSC_{0.5}$) "gold
525 standard" criterion was used to estimate the resolution of the final 3D reconstructions [86].
526 The global resolution of the entire virion density map was determined to be 4.2 Å, without
527 applying a mask. Local resolution was estimated as previously described [47]. Map
528 segmentation was performed using the Segger tool in Chimera [87]. Phenix was used for
529 autosharpening, atomic model fitting, and map validation for the segmented coat and Dec
530 densities [88]. A portion of the native phage L capsid map (segmented coat and Dec
531 density) has been deposited in the EMDB database (accession number EMD-9392).
532 Graphical representations were generated using the UCSF Chimera visualization software
533 package [87].
534
535 **NMR characterization of the structure and dynamics of monomeric Dec:** Samples of
536 recombinant Dec enriched in ^{15}N, ^{13}C and ^{2}H isotopes for NMR studies were expressed in *E.*
537 *coli* and purified as described [52]. To obtain samples suitable for NMR, 0.3 to 0.5 mM Dec
538 was unfolded to pH 2 for 20 min, followed by refolding to pH 4.0 in 20 mM sodium acetate
539 buffer containing 50 mM NaCl and 1 mM EDTA. The acid-unfolding/refolding procedure
540 converted Dec to a monomer as monitored by native gel electrophoresis and size exclusion
541 chromatography. All NMR data were collected for samples held at a temperature of 33 ºC.
542 Virtually complete NMR assignments for monomeric Dec (> 98% of backbone resonances)
543 were obtained using a suite of 3D NMR experiments [52] and have been deposited in the

544 Biological Magnetic Resonance Bank (http://www.bmrb.wisc.edu/) with the accession
545 number 27435.

546 NMR structures for Dec were calculated with the program ARIA v. 2.3.1 [53] using
547 the experimental restraints summarized in Table 1. Backbone (ϕ,ψ) and side chain (χ1)
548 torsion angles were calculated from assigned HN, N, Hα, Cα, Cβ, and CO NMR chemical
549 shifts using the program TALOS-N [54]. NOE-based distance restraints were obtained from
550 3D ^{15}N- and ^{13}C-NOESY experiments collected on ^{15}N/^{13}C-labeled Dec samples, with or
551 without 50% fractional deuteration. The NOESY experiments were collected on an 800 MHz
552 spectrometer equipped with a cryogenic probe, using a mixing time of 100 ms. Hydrogen
553 bond restraints were included based on H-bond donors and acceptors identified in a long-
554 range HNCO experiment [89] recorded on a ^{2}H,^{13}C,^{15}N triple-labeled Dec sample in TROSY
555 mode at 800 MHz, and H-bond donors inferred from amide proton protection in ^{1}H to ^{2}H
556 hydrogen exchange experiments. Water refinement in the program ARIA [53] was used as a
557 final optimization step for the NMR structures.

558 Backbone dynamics of Dec were characterized using ^{15}N NMR R1, R2, and ^{1}H-^{15}N
559 NOE relaxation data recorded at 800 MHz. R1 rates were obtained using interleaved
560 relaxation delays of 0.05, 0.13, 0.21, 0.49, 0.57, 0.71 and 0.99 s. R2 rates were determined
561 using interleaved relaxation delays of 0.01, 0.03, 0.05, 0.07, 0.09, 0.11, and 0.15 s. A 2 s
562 pre-acquisition delay was used for recovery to thermal equilibrium. ^{1}H-^{15}N NOE values were
563 determined from the ratio of crosspeak intensities in a spectrum for which the proton signals
564 were saturated for 2.5 s and a control spectrum in which the saturation period was replaced
565 by a pre-acquisition delay of equivalent length. The processing and analysis of relaxation
566 parameters was done according to published protocols [57]. Model-free analyses [90] of the
567 ^{15}N relaxation data were performed with the program Tensor2 [91], yielding an optimal global
568 isotropic rotational correlation time of 7.4 ns.
569

570 **Flexible fitting of coat protein and Dec into the cryo-EM map:** Initial structures of the
571 capsid proteins were built via homology modeling based on the available structure for P22
572 (PDB ID 5UU5 [49]). Using the symmetry operations in the PDB structure, 1/8th of the capsid
573 was constructed to cover the entire cryo-EM density map for phage L. To obtain an initial
574 structure, the entire capsid complex was fitted via rigid-body docking to the density map
575 using UCSF Chimera [87].

576 After docking and refining the NMR-derived N-terminal OB-fold of Dec, a model for
577 the helix spanning residues 78 to 86, and a linker was added to cover residues 87-92 before
578 connecting with a homology model for the C-terminus based on a fragment from the
579 bacteriophage T4 proximal long tail fiber protein gp34 (PDB ID: 4UXE [59]). The EM density
580 lacks sufficient resolution for reliably modeling the C-terminal part of Dec in terms of side
581 chain orientations but indicates a barrel-shaped structure consistent with a β-helix seen in
582 many bacteriophage tail structures. The modeled β-helix is also consistent with the β-sheet
583 secondary structure predicted for the C-terminus of Dec from its sequence [34,36,52]. The
584 selection of this structure as a template was based on the dimension of the β-helix that was
585 narrower than most β-helices found in other tail structures, and in better agreement with the
586 EM density. The complete model of the Dec trimer was then optimized against the EM
587 density via flexible fitting using the MDFF protocol within NAMD [92]. During the flexible fit,
588 residues 1-77 were restrained at Cα and Cβ positions and the helices in each subunit
589 spanning from 79-86 as well as the trimeric β-helix involving residues above 104 were
590 internally restrained Cα positions. This allowed the C-terminal part of the trimer to move
591 separately from the N-terminus to find the best fit to the EM density while preserving the
592 secondary structure motifs. We note, that while the model for the N-terminal part of Dec is
593 supported by NMR data and a good fit to the relatively high resolution EM density, the model
594 for the C-terminus is speculative due to a lack of high-resolution experimental data,
595 therefore we only show the Cα backbone.

Acknowledgements: We thank Timothy S. Baker (University of California, San Diego), Gabriel C. Lander and John E. Johnson (The Scripps Research Institute) for advice and support during the preliminary phase of this project, Giovanni Cardone for support in the local resolution analysis, Prof. Angela Gronenborn (U. Pittsburgh School of Medicine) for useful discussion, and Anne R. Kaplan for help with NMR structure calculations of Dec. This material is based upon work supported by the AAAS Marion Milligan Mason Award for Women in the Chemical Sciences to KNP, by grants NIH GM084953 and GM126948 to MF, NIH grant R01 GM076661 and a grant from the UConn Research Excellence Program to CMT and ATA. High-resolution cryo-electron microscopy data were collected at Florida State University, and the FSU facility is supported by the following grants: S10 OD018142 and S10 RR025080 under PI Ken Taylor. We would like to thank Kaillathe "Pappan" Padmanabhan for his assistance in the setup and maintenance of our computational resources. We thank Dr. Sundharraman Subramanian for help with COOT. Finally, we gratefully acknowledge the NVIDIA Corporation with the donation of the Titan V GPU used for this research.

Competing Interests

The authors have no competing interests to declare.

References:

1. Bamford DH, Grimes JM, Stuart DI (2005) What does structure tell us about virus evolution? Curr Opin Struct Biol 15: 655-663.
2. Caspar DLD, Klug A (1962) Physical principles in the construction of regular viruses. Cold Spring Harbor Symp Quant Biol 27: 1-24.
3. Bergh O, Borsheim KY, Bratbak G, Heldal M (1989) High abundance of viruses found in aquatic environments. Nature 340: 467-468.

624 4. Wommack KE, Colwell RR (2000) Virioplankton: viruses in aquatic ecosystems. Microbiol
625 Mol Biol Rev 64: 69-114.
626 5. Hua J, Huet A, Lopez CA, Toropova K, Pope WH, Duda, RL, Hendrix, RW, Conway JF
627 (2017) Capsids and Genomes of Jumbo-Sized Bacteriophages Reveal the
628 Evolutionary Reach of the HK97 Fold. MBio 8.
629 6. Evilevitch A (2018) The mobility of packaged phage genome controls ejection dynamics.
630 Elife 7.
631 7. Kellermayer MSZ, Voros Z, Csik G, Herenyi L (2018) Forced phage uncorking: viral DNA
632 ejection triggered by a mechanically sensitive switch. Nanoscale 10: 1898-1904.
633 8. Bauer DW, Huffman JB, Homa FL, Evilevitch A (2013) Herpes virus genome, the
634 pressure is on. J Am Chem Soc 135: 11216-11221.
635 9. Bauer DW, Li D, Huffman J, Homa FL, Wilson K, Leavitt, JC, Casjens, SR, Bainers, J,
636 Evilevitch, A (2015) Exploring the Balance between DNA Pressure and Capsid
637 Stability in Herpesviruses and Phages. J Virol 89: 9288-9298.
638 10. Sharma J, Uchida M, Miettinen HM, Douglas T (2017) Modular interior loading and
639 exterior decoration of a virus-like particle. Nanoscale 9: 10420-10430.
640 11. Gelbart WM, Knobler CM (2009) Virology. Pressurized viruses. Science 323: 1682-1683.
641 12. Grayson P, Han L, Winther T, Phillips R (2007) Real-time observations of single
642 bacteriophage lambda DNA ejections in vitro. Proc Natl Acad Sci U S A 104: 14652-
643 14657.
644 13. Kindt J, Tzlil S, Ben-Shaul A, Gelbart WM (2001) DNA packaging and ejection forces in
645 bacteriophage. Proc Natl Acad Sci U S A 98: 13671-13674.
646 14. Popa MP, McKelvey TA, Hempel J, Hendrix RW (1991) Bacteriophage HK97 structure:
647 wholesale covalent cross-linking between the major head shell subunits. J Virol 65:
648 3227-3237.
649 15. Wikoff WR, Duda RL, Hendrix RW, Johnson JE (1998) Crystallization and preliminary X-
650 ray analysis of the dsDNA bacteriophage HK97 mature empty capsid. Virology 243:
651 113-118.
652 16. Duda RL (1998) Protein chainmail: catenated protein in viral capsids. Cell 94: 55-60.
653 17. Sternberg N, Weisberg R (1977) Packaging of coliphage lambda DNA. II. The role of the
654 gene D protein. J Mol Biol 117: 733-759.
655 18. Imber R, Tsugita A, Wurtz M, Hohn T (1980) Outer surface protein of bacteriophage
656 lambda. J Mol Biol 139: 277-295.
657 19. Dokland T, Murialdo H (1993) Structural transitions during maturation of bacteriophage
658 lambda capsids. J Mol Biol 233: 682-694.
659 20. Lander GC, Evilevitch A, Jeemaeva M, Potter CS, Carragher B, Johnson JE (2008)
660 Bacteriophage lambda stabilization by auxiliary protein gpD: timing location, and
661 mechanism of attachment determined by cryo-EM. Structure 16: 1399-1406.
662 21. Yang Q, Maluf NK, Catalano CE (2008) Packaging of a unit-length viral genome: the role
663 of nucleotides and the gpD decoration protein in stable nucleocapsid assembly in
664 bacteriophage lambda. J Mol Biol 383: 1037-1048.
665 22. Parent KN, Khayat R, Tu LH, Suhanovsky MM, Cortines JR, Teschke CM, Johnson JE,
666 Baker TS (2010) P22 coat protein structures reveal a novel mechanism for capsid
667 maturation: Stability without auxiliary proteins or chemical crosslinks. Structure 18:
668 390-410.
669 23. Chen DH, Baker ML, Hryc CF, DiMaio F, Jakana J, Wu W, Dougherty M, Haase-
670 Pettingell C, Schmid MF, Jiang W, Baker D, King JA, Chiu W (2011) Structural basis
671 for scaffolding-mediated assembly and maturation of a dsDNA virus. Proc Natl Acad
672 Sci U S A 108: 1355-1360.

673 24. Spilman MS, Dearborn AD, Chang JR, Damle PK, Christie GE, Dokland T (2011) A
674 conformational switch involved in maturation of *Staphylococcus aureus*
675 bacteriophage 80α capsids. Journal of Molecular Biology 405: 863-876.
676 25. Parent KN, Gilcrease EB, Casjens SR, Baker TS (2012) Structural evolution of the P22-
677 like phages: Comparison of Sf6 and P22 procapsid and virion architectures. Virology
678 427: 177-188.
679 26. Parent KN, Tang J, Cardone G, Gilcrease EB, Janssen ME, Olson NH, Casjens SR,
680 Baker TS (2014) Three-dimensional reconstructions of the bacteriophage CUS-3
681 virion reveal a conserved I-domain but a distinct tailspike receptor-binding domain.
682 Virology Accepted.
683 27. Casjens SR, Thuman-Commike PA (2011) Evolution of mosaically related tailed
684 bacteriophage genomes seen through the lens of phage P22 virion assembly.
685 Virology 411: 393-415.
686 28. Parent KN, Zlotnick A, Teschke CM (2006) Quantitative analysis of multi-component
687 spherical virus assembly: Scaffolding protein contributes to the global stability of
688 phage P22 procapsids. J Mol Biol 359: 1097-1106.
689 29. Teschke CM, Parent KN (2010) 'Let the phage do the work': Using the phage P22 coat
690 protein structure as a framework to understand its folding and assembly mutants.
691 Virology 401: 119-130.
692 30. Parent KN, Schrad JR, Cingolani G (2018) Breaking Symmetry in Viral Icosahedral
693 Capsids as Seen through the Lenses of X-ray Crystallography and Cryo-Electron
694 Microscopy. Viruses 10.
695 31. Hendrix RW (2002) Bacteriophages: evolution of the majority. Theor Popul Biol 61: 471-
696 480.
697 32. Baker ML, Jiang W, Rixon FJ, Chiu W (2005) Common ancestry of herpesviruses and
698 tailed DNA bacteriophages. J Virol 79: 14967-14970.
699 33. Gilcrease EB, Winn-Stapley DA, Hewitt FC, Joss L, Casjens SR (2005) Nucleotide
700 sequence of the head assembly gene cluster of bacteriophage L and decoration
701 protein characterization. J Bacteriol 187: 2050-2057.
702 34. Tang L, Gilcrease EB, Casjens SR, Johnson JE (2006) Highly discriminatory binding of
703 capsid cementing protiens in bacteriophage L. Structure 14: 837-845.
704 35. Veesler D, Johnson JE (2012) Virus maturation. Annu Rev Biophys 41: 473-496.
705 36. Parent KN, Deedas CT, Egelman EH, Casjens SR, Baker TS, Teschke CM (2012)
706 Stepwise molecular display utilizing icosahedral and helical complexes of phage coat
707 and decoration proteins in the development of robust nanoscale display vehicles.
708 Biomaterials 33: 5628-5637.
709 37. Tao P, Zhu J, Mahalingam M, Batra H, Rao VB (2018) Bacteriophage T4 nanoparticles
710 for vaccine delivery against infectious diseases. Adv Drug Deliv Rev.
711 38. Serwer P, Wright ET (2018) Nanomedicine and Phage Capsids. Viruses 10.
712 39. Tao P, Mahalingam M, Zhu J, Moayeri M, Sha J, Lawrence WS, Leppla SH, Chopra AK,
713 Rao VB (2018) A Bacteriophage T4 Nanoparticle-Based Dual Vaccine against
714 Anthrax and Plague. MBio 9.
715 40. Asija K, Teschke CM (2018) Lessons from bacteriophages part 1: Deriving utility from
716 protein structure, function, and evolution. PLoS Pathog 14: e1006971.
717 41. Douglas T, Young M (2006) Viruses: making friends with old foes. Science 312: 873-875.
718 42. Schwarz B, Madden P, Avera J, Gordon B, Larson K, Miettinen HM, Uchida M, LaFrance
719 B, Basu G, Rynda-Apple A, Douglas T (2015) Symmetry Controlled, Genetic
720 Presentation of Bioactive Proteins on the P22 Virus-like Particle Using an External
721 Decoration Protein. ACS Nano 9: 9134-9147.

722 43. McCoy K, Uchida M, Lee B, Douglas T (2018) Templated Assembly of a Functional
723 Ordered Protein Macromolecular Framework from P22 Virus-like Particles. ACS
724 Nano 12: 3541-3550.
725 44. Catalano CE (2018) Bacteriophage lambda: The path from biology to theranostic agent.
726 Wiley Interdiscip Rev Nanomed Nanobiotechnol.
727 45. Suhanovsky MM, Teschke CM (2015) Nature's favorite building block: Deciphering
728 folding and capsid assembly of proteins with the HK97-fold. Virology 479-480: 487-
729 497.
730 46. Murzin AG (1993) OB(oligonucleotide/oligosaccharide binding)-fold: common structural
731 and functional solution for non-homologous sequences. EMBO J 12: 861-867.
732 47. Cardone G, Heymann JB, Steven AC (2013) One number does not fit all: mapping local
733 variations in resolution in cryo-EM reconstructions. J Struct Biol 184: 226-236.
734 48. Pintilie GD, Zhang J, Goddard TD, Chiu W, Gossard DC (2010) Quantitative analysis of
735 cryo-EM density map segmentation by watershed and scale-space filtering, and
736 fitting of structures by alignment to regions. Journal of structural biology 170: 427-
737 438.
738 49. Hryc CF, Chen DH, Afonine PV, Jakana J, Wang Z, Haase-Pettingell C, Jiang W, Adams
739 PD, King JA, Schmid MF, Chiu W (2017) Accurate model annotation of a near-
740 atomic resolution cryo-EM map. Proc Natl Acad Sci U S A 114: 3103-3108.
741 50. Rizzo AA, Suhanovsky MM, Baker ML, Fraser LC, Jones LM, Rempel DL, Gross ML,
742 Chius W, Alexandrescu AT, Teschke CM (2014) Multiple functional roles of the
743 accessory I-domain of bacteriophage P22 coat protein revealed by NMR structure
744 and CryoEM modeling. Structure 22: 830-841.
745 51. Eyrich VA, Marti-Renom MA, Przybylski D, Madhusudhan MS, Fiser A, Pazos F,
746 Valencia A, Sali A, Rost B (2001) EVA: continuous automatic evaluation of protein
747 structure prediction servers. Bioinformatics 17: 1242-1243.
748 52. Newcomer RL, Belato HB, Teschke CM, Alexandrescu AT (2018) NMR assignments of
749 the phage-cementing protein Decorator. Biomol NMR Assign.
750 53. Bardiaux B, Malliavin T, Nilges M (2012) ARIA for solution and solid-state NMR.
751 Methods Mol Biol 831: 453-483.
752 54. Shen Y, Vernon R, Baker D, Bax A (2009) De novo protein structure generation from
753 incomplete chemical shift assignments. J Biomol NMR 43: 63-78.
754 55. Holm L, Rosenstrom P (2010) Dali server: conservation mapping in 3D. Nucleic Acids
755 Res 38: W545-549.
756 56. Alexandrescu AT, Gittis AG, Abeygunawardana C, Shortle D (1995) NMR structure of a
757 stable "OB-fold" sub-domain isolated from staphylococcal nuclease. J Mol Biol 250:
758 134-143.
759 57. Alexandrescu AT, Shortle D (1994) Backbone dynamics of a highly disordered 131
760 residue fragment of staphylococcal nuclease. J Mol Biol 242: 527-546.
761 58. Guardino KM, Sheftic SR, Slattery RE, Alexandrescu AT (2009) Relative stabilities of
762 conserved and non-conserved structures in the OB-fold superfamily. Int J Mol Sci 10:
763 2412-2430.
764 59. Granell M, Namura M, Alvira S, Kanamaru S, van Raaij MJ (2017) Crystal Structure of
765 the Carboxy-Terminal Region of the Bacteriophage T4 Proximal Long Tail Fiber
766 Protein Gp34. Viruses 9.
767 60. Parent KN, Suhanovsky MM, Teschke CM (2007) Phage P22 procapsids equilibrate with
768 free coat protein subunits. J Mol Biol 365: 513-522.
769 61. Suhanovsky MM, Parent KN, Dunn SE, Baker TS, Teschke CM (2010) Determinants of
770 bacteriophage P22 polyhead formation: the role of coat protein flexibilty in
771 conformational switching. Mol Micro 77: 1568-1582.

772 62. Suhanovsky MM, Teschke CM (2013) An intramolecular chaperone inserted in
773 bacteriophage P22 coat protein mediates its chaperonin-independent folding. J Biol
774 Chem 288: 33772-33783.
775 63. Vernhes E, Renouard M, Gilquin B, Cuniasse P, Durand D, England P, Hoos S, Huet A,
776 Conway JF, Glukhov A, Ksenzencko V, Jacquet E, Nhiri N, Zinn-Justin S, Boulanger
777 P (2017) High affinity anchoring of the decoration protein pb10 onto the
778 bacteriophage T5 capsid. Sci Rep 7: 41662.
779 64. Doore SM, Schrad JR, Dean WF, Dover JA, Parent KN (2018) Shigella Phages Isolated
780 during a Dysentery Outbreak Reveal Uncommon Structures and Broad Species
781 Diversity. J Virol 92.
782 65. Sathaliyawala T, Islam MZ, Li Q, Fokine A, Rossmann MG, Rao VB (2010) Functional
783 analysis of the highly antigenic outer capsid protein, Hoc, a virus decoration protein
784 from T4-like bacteriophages. Mol Microbiol 77: 444-455.
785 66. Fokine A, Islam MZ, Zhang Z, Bowman VD, Rao VB, Rossmann MG (2011) Structure of
786 the three N-terminal immunoglobulin domains of the highly immunogenic outer
787 capsid protein from a T4-like bacteriophage. J Virol 85: 8141-8148.
788 67. Choi KH, McPartland J, Kaganman I, Bowman VD, Rothman-Denes LB, Rossmann MG
789 (2008) Insight into DNA and protein transport in double-stranded DNA viruses: the
790 structure of bacteriophage N4. J Mol Biol 378: 726-736.
791 68. Wang Z, Hardies SC, Fokine A, Klose T, Jiang W, Cho BC, Rossmann MG (2018)
792 Structure of the Marine Siphovirus TW1: Evolution of Capsid-Stabilizing Proteins and
793 Tail Spikes. Structure 26: 238-248 e233.
794 69. Qin L, Fokine A, O'Donnell E, Rao VB, Rossmann MG (2010) Structure of the small
795 outer capsid protein, Soc: a clamp for stabilizing capsids of T4-like phages. J Mol
796 Biol 395: 728-741.
797 70. Stone NP, Hilbert BJ, Hidalgo D, Halloran KT, Lee J, Sontheimer EJ, Kelch BA (2018) A
798 Hyperthermophilic Phage Decoration Protein Suggests Common Evolutionary Origin
799 with Herpesvirus Triplex Proteins and an Anti-CRISPR Protein. Structure 26: 936-
800 947 e933.
801 71. Zhou ZH, Prasad BV, Jakana J, Rixon FJ, Chiu W (1994) Protein subunit structures in
802 the herpes simplex virus A-capsid determined from 400 kV spot-scan electron
803 cryomicroscopy. J Mol Biol 242: 456-469.
804 72. Heming JD, Conway JF, Homa FL (2017) Herpesvirus Capsid Assembly and DNA
805 Packaging. Adv Anat Embryol Cell Biol 223: 119-142.
806 73. Shivachandra SB, Rao M, Janosi L, Sathaliyawala T, Matyas GR, Alving CR, Leppla,
807 Rao VB (2006) In vitro binding of anthrax protective antigen on bacteriophage T4
808 capsid surface through Hoc-capsid interactions: a strategy for efficient display of
809 large full-length proteins. Virology 345: 190-198.
810 74. Teschke CM, McGough A, Thuman-Commike PA (2003) Penton release from P22 heat-
811 expanded capsids suggests importance of stabilizing penton-hexon interactions
812 during capsid maturation. Biophysical Journal 84: 2585-2592.
813 75. Llauro A, Schwarz B, Koliyatt R, de Pablo PJ, Douglas T (2016) Tuning Viral Capsid
814 Nanoparticle Stability with Symmetrical Morphogenesis. ACS Nano 10: 8465-8473.
815 76. Lambert S, Yang Q, De Angeles R, Chang JR, Ortega M, Davis C, Catalano CE (2017)
816 Molecular Dissection of the Forces Responsible for Viral Capsid Assembly and
817 Stabilization by Decoration Proteins. Biochemistry 56: 767-778.
818 77. Yang F, Forrer P, Dauter Z, Conway JF, Cheng N, Cerritello ME, Steven AC, Pluckthun
819 A, Wlodawer A (2000) Novel fold and capsid-binding properties of the lambda-phage
820 display platform protein gpD. Nat Struct Biol 7: 230-237.
821 78. Forrer P, Chang C, Ott D, Wlodawer A, Pluckthun A (2004) Kinetic stability and crystal
822 structure of the viral capsid protein SHP. J Mol Biol 344: 179-193.

79. D'Lima NG, Teschke CM (2015) A Molecular Staple: D-Loops in the I Domain of Bacteriophage P22 Coat Protein Make Important Intercapsomer Contacts Required for Procapsid Assembly. J Virol 89: 10569-10579.
80. Baker TS, Olson NH, Fuller SD (1999) Adding the third dimension to virus life cycles: three-dimensional reconstruction of icosahedral viruses from cryo-electron micrographs. [erratum appears in Microbiol Mol Biol Rev 2000 Mar;64(1):237.]. Microbiology & Molecular Biology Reviews 63: 862-922.
81. Mastronarde DN (2005) Automated electron microscope tomography using robust prediction of specimen movements. J Struct Biol 1: 36-51.
82. Wang Z, Hryc C, Bammes B, Afonine PV, Jakana J, Chen DH, Liu X, Kao C, Ludtke SJ, Schmid MF, Adams PD, Chiu W (2014) An atomic model of brome mosaic virus using direct electron detection and real-space optimization. Nature Communications 5: 4808.
83. Yan X, Dryden KA, Tang J, Baker TS (2007) Ab initio random model method facilitates 3D reconstruction of icosahedral particles. J Struct Biol 157: 211-225.
84. Yan X, Sinkovits RS, Baker TS (2007) AUTO3DEM-an automated and high throughput program for image reconstruction of icosahedral particles. J Struct Biol 157: 73-82.
85. Bowman VD, Chase ES, Franz AW, Chipman PR, Zhang X, Perry KL, Baker TS, Smith TJ (2002) An antibody to the putative aphid recognition site on cucumber mosaic virus recognizes pentons but not hexons. J Virol 76: 12250-12258.
86. Pintilie G, Chen DH, Haase-Pettingell CA, King JA, Chiu W (2016) Resolution and Probabilistic Models of Components in CryoEM Maps of Mature P22 Bacteriophage. Biophys J 110: 827-839.
87. Goddard TD, Huang CC, Ferrin TE (2007) Visualizing density maps with UCSF Chimera. J Struct Biol 157: 281-287.
88. Afonine PV, Klaholz BP, Moriarty NW, Poon BK, Sobolev OV, Terwilliger TC, Adams PD, Urzhumtsev A (2018) New tools for the analysis and validation of cryo-EM maps and atomic models. Acta Crystallogr D Struct Biol 74: 814-840.
89. Cordier F, Grzesiek S (1999) Direct observation of hydrogen bonds in proteins by interresidue 3HJNC' scalar couplings. J Am Chem Soc: 1601-1602.
90. Lipari G, Szabo, A. (1982) Model-Free Approach to the Interpretation of Nuclear Magnetic Resonance Relaxation in Macromolecules. 1. Theory and Validity. J Am Chem Soc 104: 4546-4559.
91. Dosset P, Hus JC, Blackledge M, Marion D (2000) Efficient analysis of macromolecular rotational diffusion from heteronuclear relaxation data. J Biomol NMR 16: 23-28.
92. Trabuco LG, Villa E, Mitra K, Frank J, Schulten K (2008) Flexible fitting of atomic structures into electron microscopy maps using molecular dynamics. Structure 16: 673-683.
93. Henderson R, Sali A, Baker ML, Carragher B, Devkota B, Downing KH, Egelman EH, Feng Z, Frank J, Grigorieff N, Jiang W, Ludtke SJ, Medalia O, Penczek PA, Rosenthal PB, Rossmann MG, Schmid MF, Schroder GF, Steven AC, Stokes DL, Westbrook JD, Wriggers W, Yang H, Young J, Berman HM, Chiu W, Kleywegt GJ, Lawson CL (2012) Outcome of the first electron microscopy validation task force meeting. Structure 20: 205-214.
94. Kumar GS, Clarkson MW, Kunze MBA, Granata D, Wand AJ, Lindorff-Lanrsen K, Page R, Peti W (2018) Dynamic activation and regulation of the mitogen-activated protein kinase p38. Proc Natl Acad Sci U S A 115: 4655-4660.

873 **TABLES AND FIGURE LEGENDS**

874 **Tables:**

875

876 **Table 1: Cryo-EM data collection and model refinement statistics**
877

Data collection	
EM equipment	FEI Titan Krios
Voltage (kV)	300
Detector	DE-20
Pixel size (Å)	1.26
Electron Dose ($e^-/Å^2$)	27
Defocus range (μm)	0.35 - 2.49

Reconstruction	
Software	AUTO3DEM
Number of particles	7,879
Symmetry	532
Map resolution (Å) at FSC = 0.143	4.2

Model building and Refinement	
Software	COOT, Phenix

Model Statistics and Validation	**Coat**	**Dec**
No. protein chains in ASU	7	3
No. residues per protein	430	134
Model resolution (Å) at FSC = 0.5	4.30	5.80
Cross-correlation coefficient (CC)	0.61	0.40
MolProbabity Score	2.21	1.93
Clashscore	2.20	0.87
R.m.s. deviations		
Bond length (Å)	0.021	0.018
Bond angle (˚)	2.62	2.21
Preferred	92.42	77.53
Allowed	5.41	13.69
Outlier	2.17	8.59

878

879

Table 2. Statistics for the top 20 NMR structures of Dec.

Experimental Restraints		
Total number of NMR restraints	1,009	
Total number of NOE distance restraints	767	
Ambiguous	73	
Unambiguous	694	
Long range (|i-j|>4)	124	
Medium range (|i-j|)≤4)	93	
Sequential (|i-j|)=1)	281	
Intra-residue NOEs	269	
Total number of dihedral restraints	174	
φ/ ψ	127	
χ_1	47	
Hydrogen bond restraints (34*2)	68	
RMSD from experimental restraints[a]		
NOE distance (Å)	0.054 ± 0.003	
Dihedral (°)	0.42 ± 0.14	
RMSD from ideal geometry		
Bonds (Å)	0.0042 ± 0.0001	
Angles (°)	0.55 ± 0.02	
Improper angles (°)	1.68 ± 0.12	
E_{L-J} (kcal/mol)	- 316 ± 44	
RMSD from mean NMR structure	Backbone [b]	All Heavy Atoms
Entire protein 1-134 (Å)	> 9.5	> 9.5
Folded regions 12-86 (Å)	1.33 ± 0.21	1.95 ± 0.32
OB-fold 18-77 (Å)	1.08 ± 0.18	1.66 ± 0.25
OB-fold 2° structure[c] (Å)	0.84 ± 0.15	1.57 ± 0.31
Procheck Ramachandran Plot Statistics[d]		
Most favored (%)	89.1	
Additionally allowed (%)	10.9	
Generously allowed (%)	0.0	
Disallowed (%)	0.0	
Quality Z Scores from PSVS[e]		
Procheck (□□□)	-2.64	
Molprobity Clash	-1.19	

[a] Structures had no NOE violations > 0.5 Å nor dihedral violations > 5 degrees.
[b] Atoms: C□, N, C, O
[c] Calculated over residues in the OB-fold portion: 21-32 (□1), 35-40 (□2), 47-50 (□3), 52-59 (□$_{OB}$), 63-68 (□4), 73-77 (□5), a total of 41 amino acids.
[d] Calculated with the PSVS server (http://psvs-1_5-dev.nesg.org) using only the folded parts of Dec (residues 12-89).

892 **Figures and Legends:**

893 **Figure 1: Cryo-EM imaging and icosahedral image reconstruction of the mature phage**
894 **L capsid.** A) Schematic of a T=7 icosahedral capsid overlaid with a black icosahedral cage.
895 The different symmetry axes are marked; two-fold by a black oval, five-fold by a black
896 pentagon, and icosahedral three-fold by a black triangle. Magenta circles highlight quasi
897 three-fold binding sites between hexamers on one icosahedral facet. The magenta quasi
898 three-folds are the preferred binding sites for Dec. Green circles highlight additional quasi
899 three-fold sites between hexons and pentons surrounding one vertex, to which Dec has
900 never been observed to bind. B) Segmented electron density for a capsid-bound Dec trimer
901 shown in a top-down view. C) Enlarged view of a quasi-3-fold symmetry axis between
902 hexons, showing the Dec binding site where the coat is segmented from the Dec trimer. The
903 density is fitted with six coat protein subunits derived from homology modeling. Three
904 orange subunits are closest to the symmetry axes and the three blue subunits are in a
905 different quasi equivalent conformation.

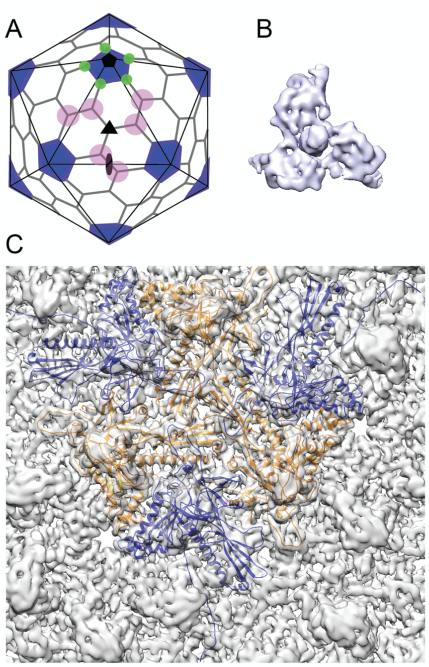

906

907 **Figure 2: NMR structure of the Dec monomer.** A) Ensemble of the 20 lowest-energy NMR
908 structures. For clarity, the disordered N- and C-termini are not shown. The folded globular
909 part of Dec has an OB-fold consisting of a β1-β3 meander (sky blue) and a β4-β5 hairpin
910 (yellow), with an α-helix (green) intervening between strands β3 and β4. Additional
911 secondary structure outside of the OB-fold incudes the short N-terminal strand β0 (dark
912 blue), and a C-terminal α-helix (pink). B) Ribbon diagram showing the structure closest to
913 the NMR average. The first 10 N-terminal residues and the last ~45 C-terminal residues,
914 which are unstructured in the Dec monomers are colored red and orange, respectively. The
915 coloring scheme for the rest of the protein in this and subsequent panels is the same as in A.
916 C) Diagram summarizing the topology and secondary structure limits of the Dec monomers.

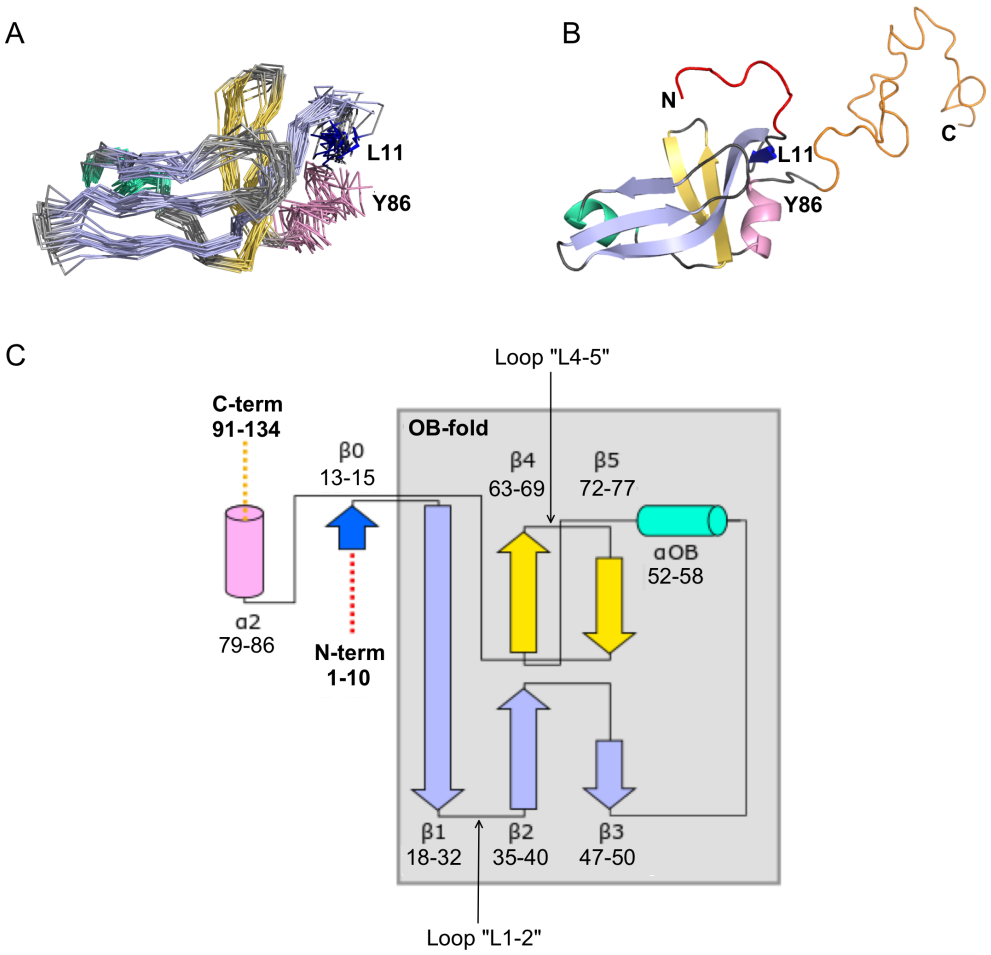

917

918

Figure 3: Dynamics of the Dec monomer. A) S^2 order parameters describing the amplitude of fast motions on the ps-ns timescale. Rigid (S^2 > 0.65), moderately flexible (0.65 ≥ S^2 > 0.55), and highly flexible (0.55 ≥ S^2) sites are indicated by black, purple, and red symbols respectively. The secondary structure of Dec is given at the top of panel A. B) Contributions to R2 relaxation from slow conformational exchange on the µs-ms timescale. Amide protons with moderate $R2_{ex}$ values smaller than 3 Hz are shown in purple, those with large contributions above 3 Hz in red. The S^2 and $R2_{ex}$ parameters were obtained from a Model-Free analysis [90] of ^{15}N R1, R2, and ^{1}H-^{15}N NOE relaxation data for Dec (Figure S3) using the program TENSOR 2.0 [91]. In C) and D) the S^2 and $R2_{ex}$ values are mapped onto the NMR structure ensembles for Dec. Residues 1-10 and 90-134 which are unfolded and thus have the lowest S^2 values, are not shown in the structures

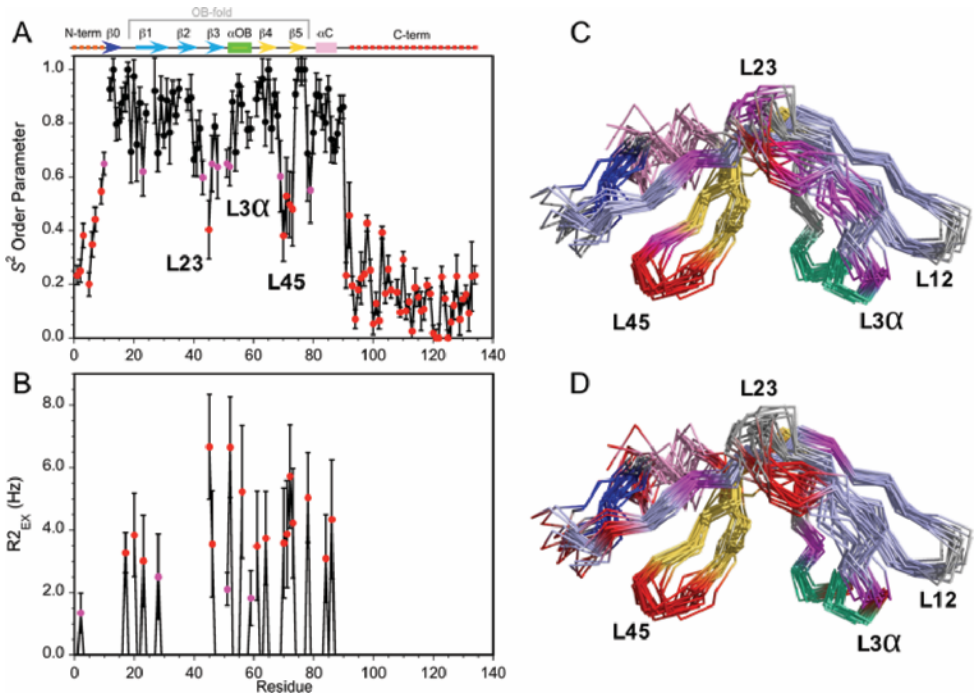

933 **Figure 4: Fitting the NMR OB-fold into the cryo-EM map and model of the trimer.** A)
934 Side B) top-down, and C) bottom-up views of the Dec trimer model fit into the cryo-EM
935 density map with individual chains colored magenta, cyan, and green.
936

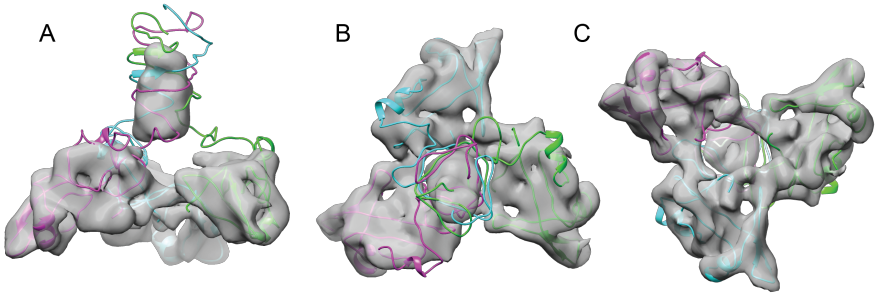

937
938
939

940 **Figure 5: Binding assays of variant coat proteins and Dec to probe the interaction**
941 **interface.** A) Coat protein subunits depicted as ribbon diagrams around a quasi three-fold
942 axis Dec binding site. Three coat subunits directly surrounding a quasi three-fold axis are
943 shown in light grey, and three neighboring coat proteins are shown in black. Residues
944 selected for mutagenesis are shown as spheres. B) Normalized binding data of the ratio of
945 variant coat protein bound to WT Dec, color-coded to match the corresponding residues in
946 panel A. C) Portions of Dec highlighting the OB-fold (residues 10-77) shown as ribbons, with
947 each monomer a different shade of blue. Residues selected for mutagenesis are shown as
948 spheres. D) Enlarged side view of the Dec cryo-EM density with the OB-fold (residues 10-
949 77) from one monomer shown as a ribbon, with the two different capsid binding sites
950 indicated. E) Normalized binding data of the ratio of WT coat protein bound to variant Dec,
951 and color-coded to match the corresponding residues in panels C and D.

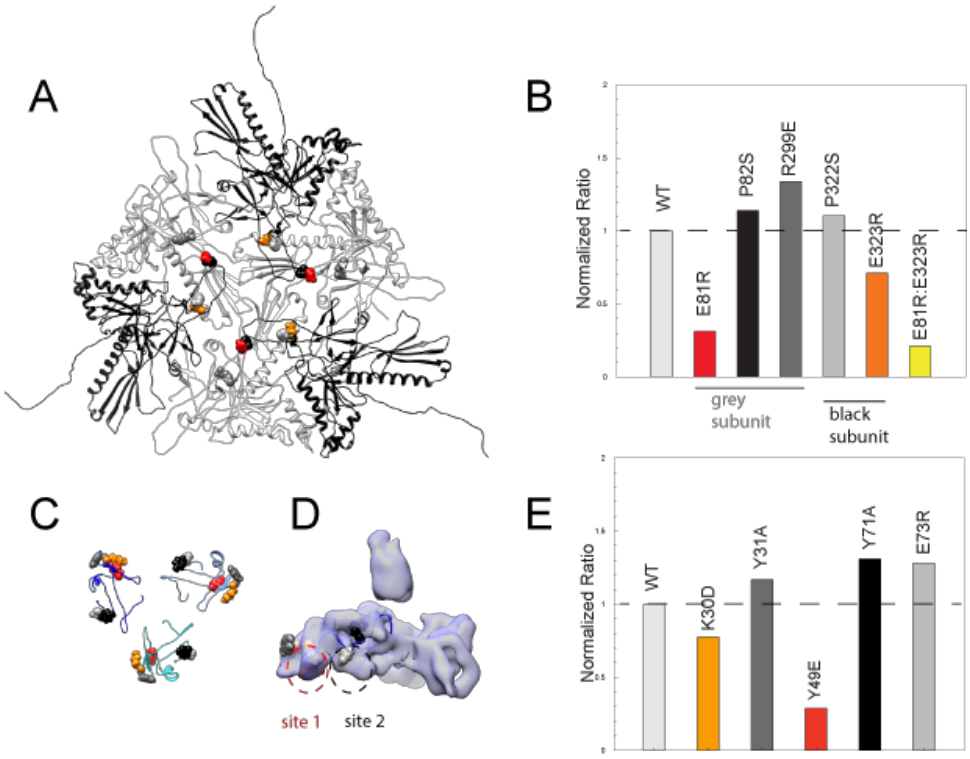

952

953 **Figure 6: Comparison of Dec binding residues at various three fold symmetry sites on**
954 **the phage L capsid.** The topology of six coat protein subunits surrounding the different
955 three fold symmetry axes were compared using the Match tool in Chimera. The quasi three-
956 fold site between coat protein hexamers (magenta) that binds a Dec trimer was chosen as
957 the reference structure and aligned to the three-fold site between a pentamer and
958 neighboring hexamers (green) that does not bind Dec. The cartoon schematic below shows
959 the location of residue E81 with a small magenta circle on three coat protein subunits that
960 comprise the Dec binding interface (label "A" designates the specific coat protein subunit
961 used for anchoring the structures in Chimera). The relative displacement of E81 in subunits
962 labeled "1" or "2" when in an icosahedral three-fold or the quasi three-fold surrounding
963 pentamers was measured and the distances are shown in the table. A side view of the quasi
964 three-fold site between hexamers that binds Dec (magenta) with the quasi three-fold site
965 between a penatmer and neighboring hexamers (green) is shown as a ribbon diagram. The
966 box shows an enlarged and tilted view of the binding interface with residue E81 shown as
967 spheres.
968

Site	Quasi three-fold (pentamer)	Icosahedral three-fold
1	10.4 Å	8.8 Å
2	7.3 Å	3.9 Å

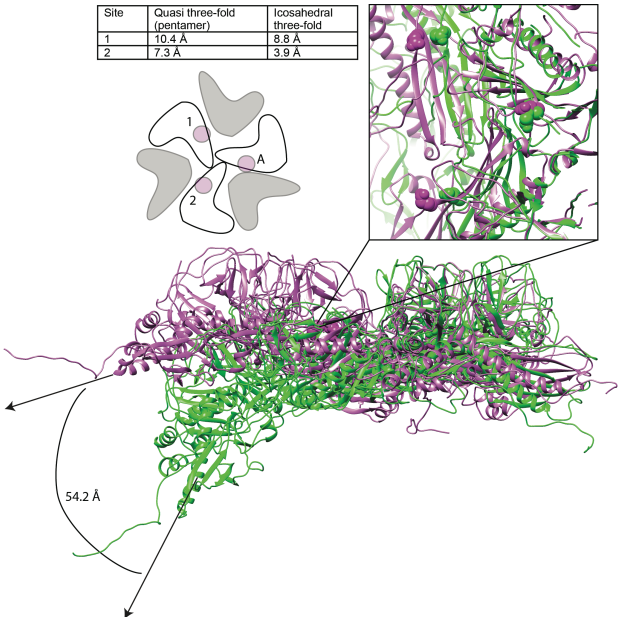

969

970 **Figure 7: Comparison of decoration proteins.** A) Side and B) top-down views of
971 decoration proteins gpD (PDB ID 1C5E), gp87 (PDB ID 6BL5) and Dec (PDB ID 6D2D).
972 Chains of each trimer are rainbow colored from N-terminus (blue) to C-terminus (red).
973

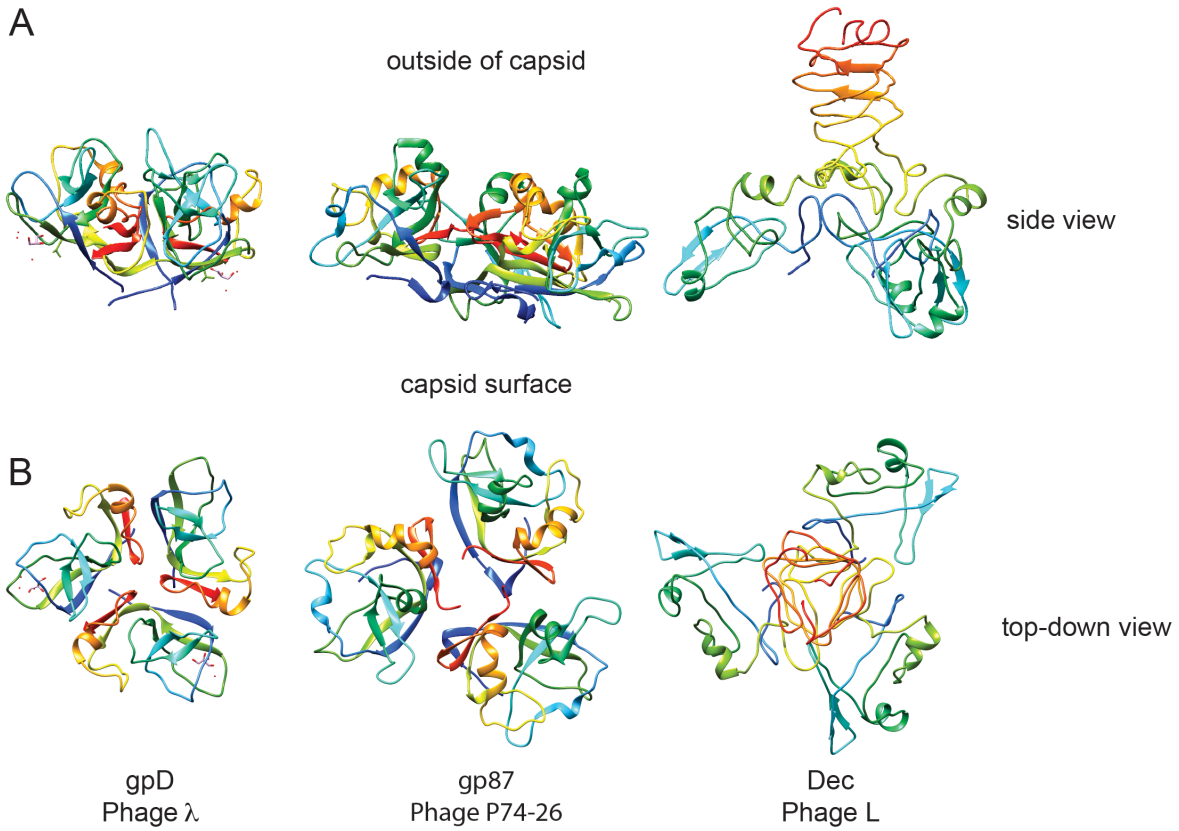

974
975

976 **Supplementary Figures/Movies Legends:**

977

978 **Figure S1): Phage L cryo-EM and 3D reconstruction data.** A) Representative micrograph
979 of frozen hydrated phage L particles. B) FSC curve with $FSC_{0.143}$ cutoff shown with a dashed
980 line. The red arrow points out the estimated global resolution of the map at 4.2 Å according
981 to the "gold standard" method [93]. C) Phage L surface rendered view, colored accorded to
982 local resolution with an octant of the virion removed to show the internal genome
983 organization. The color bar indicates resolution in Å.

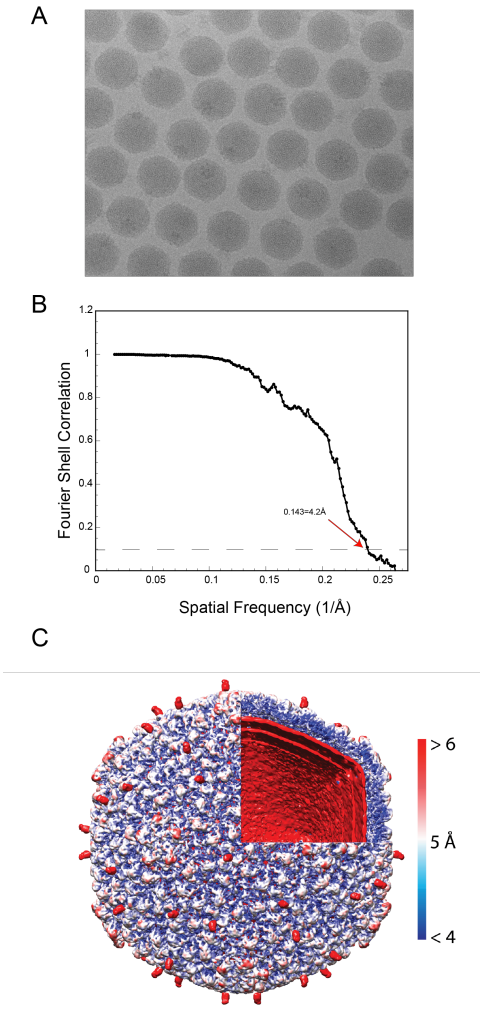

984

985 **Figure S2): Phage L coat protein subunit.** A) Single coat protein monomer color-coded
986 according to domain boundaries (N-arm in red, P-domain in green, E-loop in yellow, A-

domain in cyan, and I-domain in magenta). B) 1/8th of the capsid used for modeling with coat protein segmentation is colored in grey and the Dec segmentation is colored in lavender. Note the map is rotated to peer down a icosahedral 3-fold axis in the center of the area that was modeled to emphasize the lack of Dec density at this location.

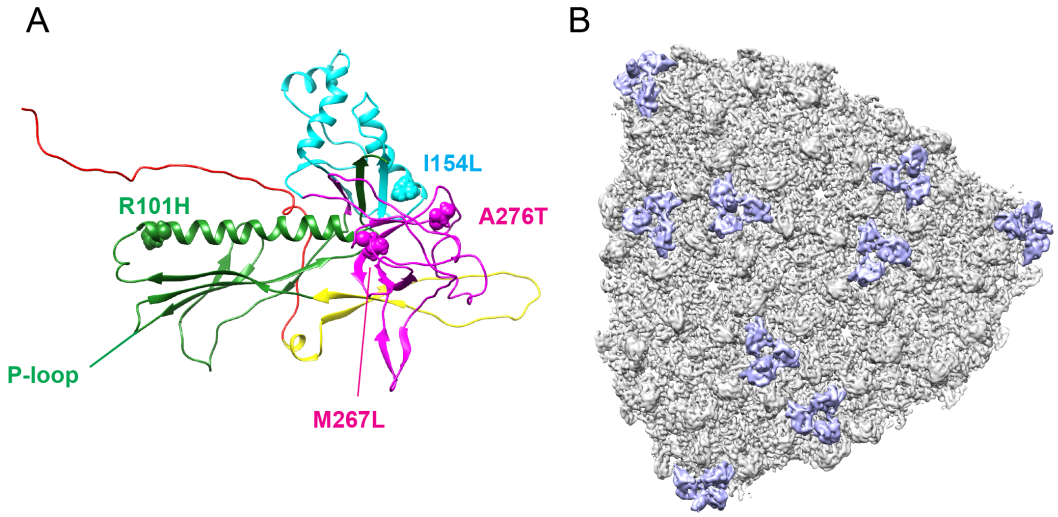

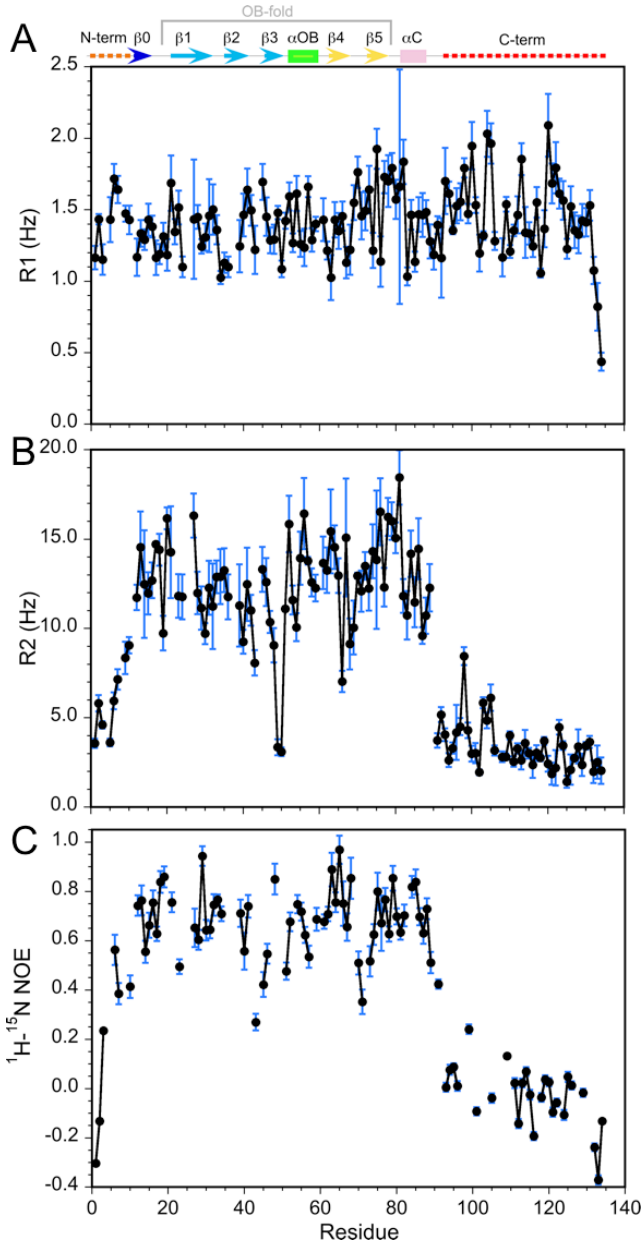

Figure S3. ^{15}N relaxation values for monomeric Dec. (A) R1, (B) R2, (C) ^{1}H-^{15}N NOE. All data were recorded at 800 MHz, with a sample temperature of 33 ºC. The secondary structure of Dec, derived from its NMR structure, is indicated at the top of the first panel. The average R2 and R1 values for the folded portions of Dec are about 13 Hz and 1.4 Hz,

1002 respectively. For comparison, a Dec trimer with the expected theoretical MW of 43 KDa
1003 should have R2 and R1 values near 50 Hz and 0.4 Hz, respectively [94]. Thus the ^{15}N
1004 relaxation data for Dec samples subjected to our unfolding/refolding protocol are more
1005 consistent with a 14.4 KDa Dec monomer than a trimer. Similarly, the Model Free analysis of
1006 the ^{15}N relaxation data gives an optimum global correlation time for isotropic rotational
1007 diffusion of 7.4 ns, consistent with a Dec monomer. For a 43 KDa trimer the value of the
1008 correlation time should be about 21 ns.
1009
1010

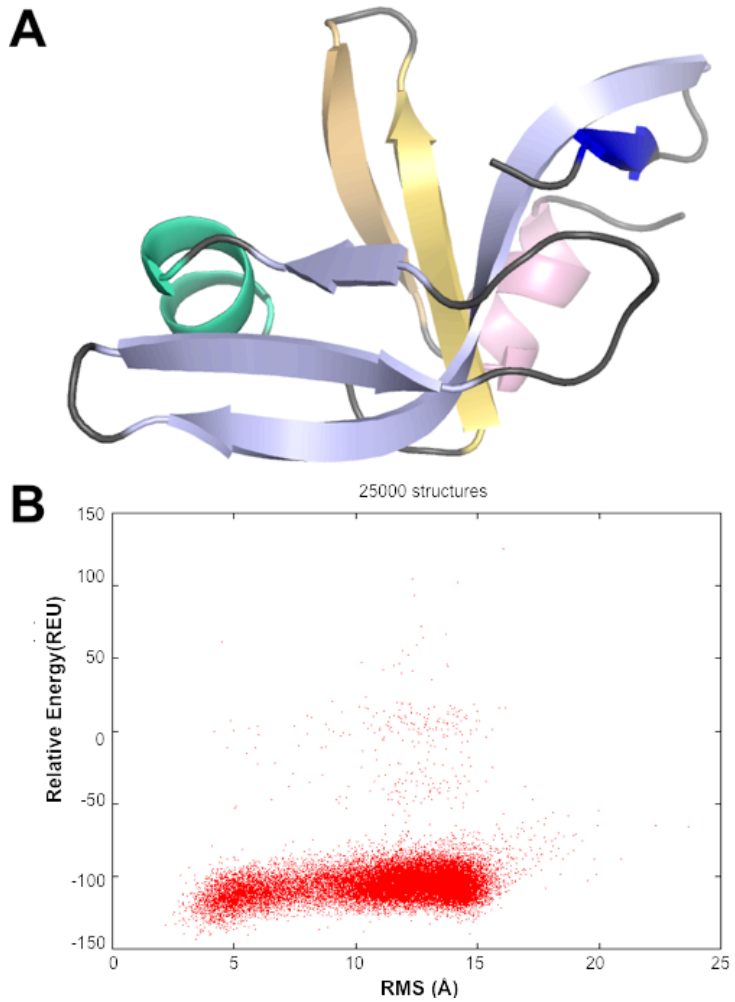

1011

1012 **Figure S4. CS-ROSETTA modeling of the Dec monomer structure. (A)** The lowest
1013 energy model based on the assigned NMR chemical shifts of Dec [52] has an OB-fold
1014 topology. Only residues 10-88 were included in the CS-ROSETTA simulations [54], since
1015 the program predicted that residues 1-9 and 89-134 are disordered, based on the assigned
1016 NMR chemical shifts. The 5-stranded, Greek Key β-barrel OB-fold motif [46] is formed from
1017 a β1-b3 meander (light blue) and a β4-β5 hairpin (yellow), with an α-helix (green) intervening
1018 between strands β3 and β4. **(B)** Graph showing convergence of the CS-ROSETTA
1019 simulations. The statistics indicated that the CS-ROSETTA simulations did not fully
1020 converge. In spite of this, nine of the top ten lowest energy structures had an OB-fold
1021 structure with an average RMSD of 2.5 Å to the structure shown in (A).

1022 **Supplementary Movies**
1023

1024 **Movie S1**

1025 Location of the amino acid differences between phage L and P22, relative to the Dec
1026 binding interface. A single segmented Dec density is shown in lavender, and coat protein
1027 subunits that comprise the binding interface are shown as grey ribbons. The amino acid
1028 substitutions between phage L and P22 are shown as spheres color-coded to match the
1029 protein domains as shown in Figure S2: R101H (green), I154L (cyan), A276 & M267
1030 (magenta).

1031

1032

1033 **Movie S2. Key residues that modulate Dec binding affinity.** View of the binding
1034 interactions between Dec and coat protein at a quasi-three-fold symmetry axis. Coat protein
1035 is shown in grey density and Dec is shown in lavender. Six coat subunits are fit within this
1036 density and three Dec OB-fold domains from the NMR structure were fit to the Dec density.
1037 Individual protein chains are shown are ribbons; amino acid sites that were chosen for
1038 mutagenesis are shown as spheres, and color coded to match the data in Figure 5 of the
1039 main text.

1040
1041 **Movie S3. Definition of different regions of the Dec monomer NMR structure.** To
1042 illustrate the precision of the structure all 20 members of the NMR ensemble are shown. The
1043 movie than flips through the 20 individual NMR structures to show the differences in
1044 precision between the structured OB-fold component, and the unstructured N- (yellow) and
1045 C-termini (orange). In the second half of the movie, the N- and C-termini are not shown to
1046 better illustrate differences in structural definition of the OB-fold component.

1047
1048
1049